Radio detection of nebulae around four luminous blue variable stars in the Large Magellanic Cloud

C. Agliozzo,[1,2]★ G. Umana,[2] C. Trigilio,[2] C. Buemi,[2] P. Leto,[2] A. Ingallinera,[1,2]
T. Franzen[3] and A. Noriega-Crespo[4]

[1]*Dipartimento di Fisica e Astronomia, Sezione Astrofisica, Università degli studi di Catania, via S. Sofia 78, 95123 Catania, Italy*
[2]*INAF Osservatorio Astrofisico di Catania, via S. Sofia 78, 95123 Catania, Italy*
[3]*CSIRO Astronomy and Space Science, PO Box 76, Epping, NSW 1710, Australia*
[4]*Infrared Processing and Analysis Center, California Institute of Technology, Pasadena, CA 91125, USA*

ABSTRACT

The nebulae associated with four luminous blue variables (LBVs) in the Large Magellanic Cloud (LMC) have been observed at 5.5 and 9 GHz using the Australia Telescope Compact Array, and radio emission has been detected for first time in sources R127, R143, S61 and S119. The radio maps of the nebulae have an angular resolution of ∼1.5 arcsec and a sensitivity of 1.5–3.0×10^{-2} mJy beam^{-1} and show a very similar morphology to that observed in Hα. This similarity permits us to assume that the Hα emission is not affected by strong intrinsic extinction due to dust within the nebulae. We estimate the masses of ionized gas in the LBV nebulae and find values consistent with those measured in Galactic LBVs.

Key words: stars: evolution – stars: mass-loss – ISM: bubbles.

1 INTRODUCTION

The extended nebulae often observed around luminous blue variable stars (LBVs) constitute a quite typical characteristic of such evolved massive and unstable stars.

A census of known LBVs reports 35 objects in our Galaxy and 25 in the Magellanic Clouds (Clark, Larionov & Arkharov 2005; van Genderen 2001). Hence our knowledge of LBV nebulae (LBVNe) is still very limited, due in part to the small number of known LBVs and in part to the short lifetime ($t \sim 10^{-5}$–10^{-4} yr) of the LBV phase. The characterization of LBVNe is therefore fundamental to understand the evolution of massive stars, providing estimates of important physical properties such as their mass-loss history (through the determination of the kinematical age of the nebula), the origin and morphology of LBVNe and the total mass lost during the LBV phase.

Some Galactic LBVNe have recently been studied following a multiwavelength approach (Umana et al. 2011a) aimed at tracing both the gas and the dust components typically coexisting in LBVNe. Among the most interesting aspects highlighted in these studies are the following: the presence of multiple shells, which are evidence of different mass-loss episodes experienced by the star (e.g. G79.29+0.46: Jiménez-Esteban, Rizzo & Palau 2010; Umana et al. 2011b); the distribution of gas and dust, sometimes differently shaped (IRAS 18576+034: Buemi et al. 2010); the chemistry

in the nebula, sometimes rich in complex molecules such as polycyclic aromatic hydrocarbons (PAHs) (e.g. HD 168625: Umana et al. 2010); evidence that dust can survive despite the hostile environment due to UV radiation from the star.

The main mechanisms believed to lead to the formation of such nebulae are the moderate ($\dot{M} \sim 10^{-7}$–10^{-5} M$_\odot$ yr^{-1}) mass loss associated with steady stellar winds and, especially, the extreme mass-loss rates ($\dot{M} \sim 10^{-5}$–10^{-4} M$_\odot$ yr^{-1}) experienced by the star during giant eruptions, which characterize its post-main-sequence evolution. Humphreys & Davidson (1994) and later Smith & Owocki (2006) have suggested that eruptive episodes, which must form the bulk of a LBVN, are metallicity-independent. If this is true, LBVs may have had a role in the evolution of the early Universe, when massive stars would have been more numerous than in the present epoch and may have provided processed material and dust for future generations of stars.

A way to explore this possibility is to study the LBV phenomenon in environments different from the Galactic one, i.e. in galaxies with different metallicity. Considering the capabilities of the instruments available up to the present, we have begun a study of LBVNe in the Large Magellanic Cloud (LMC), which is the nearest galaxy (with an accepted distance of $D \sim 48.5$ kpc) and with half the solar metallicity ($Z \sim 0.5 Z_\odot$).

Evidence of extended nebulae around LBVs and candidate LBVs (LBVc) in the LMC has been previously reported. Weis (2003) and Weis, Duschl & Bomans (2003) performed high-resolution observations of nine LBVs and LBVc in the LMC with the Hα filter using the Wide Field Planetary Camera 2 (WFPC2) and ESO Multi-Mode

★E-mail: claudia.agliozzo@oact.inaf.it

Table 1. Observational summary.

Observation Date	ATCA Config.	Band (cm)	Total integration time (min)			
			S61	R127	R143	S119
11 Apr 18	6-km	3+6	534	534	58	59
11 Apr 21	6-km	3+6	58	59	533	536

Instrument (EMMI). In particular, they found that five of these objects show a very well-defined shell in Hα, with sizes in the range 5–18 arcsec, indicating the presence of a nebula around them.

Based on these studies we have selected a group of LVBNe that could be detected at radio wavelengths (which allows us to probe the properties of the ionized gas) through the estimation of the radio free–free emission from the observed hydrogen Hα recombination line. Here we present the first radio observations of a small subsample of these LBVNe, namely LBVc S61 and S119 plus LBVs R127 and R143.

This paper is organized as follows: after an explanation of the observation and data-reduction strategies (Section 2) we compare the radio free–free continuum emission with that of Hα from the morphological and photometric points of view (Sections 3 and 4). In Section 4 we also estimate some physical parameters related to the nebulae and in Section 5 we present our final remarks.

2 OBSERVATIONS AND DATA REDUCTION

2.1 ATCA observations

Radio continuum observations were carried out on 2011 April 18 and 20 at the Australia Telescope Compact Array (ATCA), using the interferometer in the 6-km configuration. Data were acquired with the new back-end system Compact Array Broadband Backend (CABB), with a maximum bandwidth of 2 GHz in the 3+6 cm band. The observations consisted of 15-min scans on the target, preceded and followed by 2-min scans on the phase calibrator (0530−727), for a total of ∼10 h on-source integration time. In order to achieve the best $u − v$ coverage, the scans were distributed over 12 values of hour angle. We used 1934−638 for the bandpass and flux calibration. Table 1 summarizes the observations.

Data sets were separately edited and reduced by using the MIRIAD software package (Sault, Teuben & Wright 1995). After applying the bandpass and time-based gain corrections, the calibrated visibilities were imported into the CASA package[1] and processed for imaging, using the task CLEAN and performing a natural weighting to achieve the highest sensitivity. Dirty images were deconvolved using the Clark algorithm (Clark 1980). The resulting synthetic beam Θ_{syn} is typically 2.5×2.0 arcsec^2 at 5.5 GHz and 1.5×1.2 arcsec^2 at 9 GHz. For imaging R143, which is located in a very crowded region, we applied a Briggs-type weighting (parameter `robust = 0`) to minimize side-lobe contribution of the brightest sources. This choice represents a good compromise between the highest resolution and sensitivity achievable at ATCA.

The mean noise obtained for the maps is typically 1.5–2.0×10^{-2} mJy beam^{-1}, consistent with the sensitivity of the new broadband back-end system CABB at these frequencies for the integration time used.

[1] Common Astronomy Software Application, version 3.0.2.

2.2 *Hubble Space Telescope* data

In order to compare the radio morphology of the nebula with that observed at other wavelengths, Hα images have been retrieved from the STScI data archive. These images have been obtained[2] with the WFPC2 instrument using the Hα-equivalent filter F656N and reduced by the standard *Hubble Space Telescope* (*HST*) pipeline. These data had already been published by Weis (2003) and Weis et al. (2003). For each source we combined the data sets (four images with a 500-s exposure) following a standard procedure in IRAF to remove cosmic-ray artefacts and to improve the signal-to-noise ratio (S/N).

Finally, we have also recalibrated the *HST* images astrometrically using the Naval Observatory Merged Astrometric Dataset (NOMAD) catalogue (Zacharias et al. 2005) for a corrected overlay with the radio images.

3 MORPHOLOGY OF THE RADIO NEBULAE

In this section we give a morphological description of the radio emission compared with the optical (already provided by Weis 2003; Weis et al. 2003), obviously limited by the lower resolution of the radio maps. Fig. 1 shows all the maps obtained in this work, compared with the reprocessed *HST* images.

The angular sizes of the emission region were estimated by drawing a box above 3σ on the sources. The maximum and minimum sizes are hence reported in Table 2. The estimated values are consistent with the precedent measurements (e.g. Clampin et al. 1993; Smith et al. 1998; Pasquali, Nota & Clampin 1999; Weis et al. 2003; Weis 2003).

S61 is a LBV candidate (Walborn 1977, 1982), with a Hα nebula consisting of an inner brighter ring-like structure and larger diffuse emission (Weis 2003). The radio nebula here resembles the Hα one, being roughly spherical (Fig. 1). The nebula is fainter in the south-west and the emission is not homogeneous: the brightest part is in the north-east, where the gas might be thicker. Greater diffuse emission all around is evident above 3σ, as well as the outer shell seen in Hα.

R127 was classified as LBV star after it showed S-Dor-type variability (Stahl et al. 1983). Clampin et al. (1993) reported the presence of a diamond-shaped optical nebula and then the high-resolution *HST* image in Weis (2003) revealed a nearly spherical structure in the central region and fainter emission in the north and southern directions. The shell also presents two brighter rims on the east and north-west sides.

The radio nebula show two components: a thin, roughly spherical nebula, elongated in the north–south direction, and a thicker bipolar nebula, Z-pattern-shaped and centred in the optical stellar position. A hint of the central object is visible in the radio image.

R143 is a confirmed LBV (Parker et al. 1993), located in the 30 Doradus cluster. Around the star there is a nebula, elongated in the north–south direction and triangular shaped, detected with the *HST* (Smith et al. 1998; Weis 2003). As pointed out by Weis (2003), the nebula is concentrated to the west of the star, without counterpart nebular emission to the east. Four curved filaments close to R143 were noticed by Feast (1961) and then attributed to the nearby H II region by Smith et al. (1998).

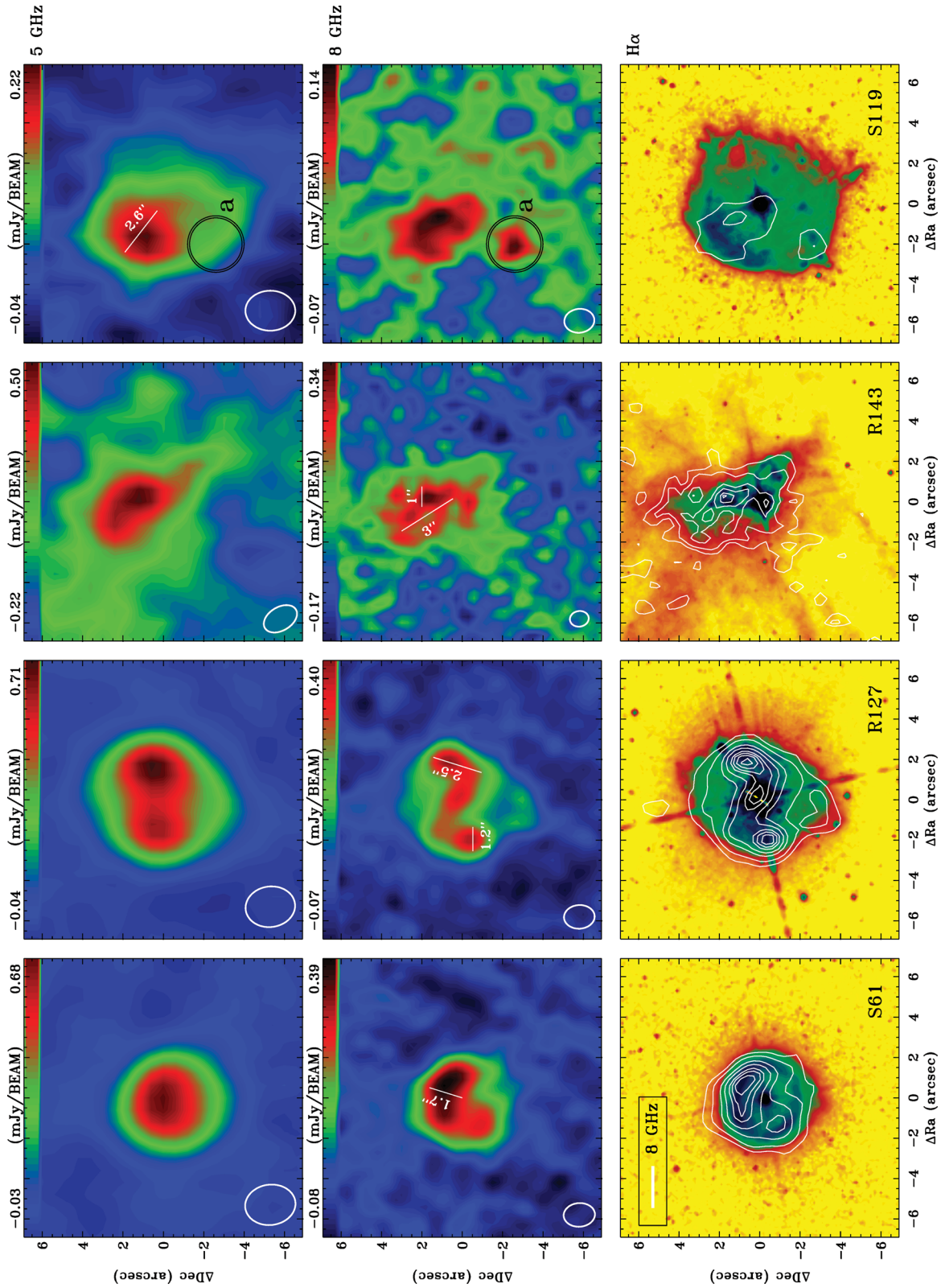[2] Proposal ID: 6540; P.I. Regina Schulte-Ladbeck.

Figure 1. Top: 5-GHz ATCA maps of S61, R127, R143 and S119 from left to right. Middle: 8-GHz ATCA maps in the same order as before. Bottom: Hα WFPC2/*HST* images overlaid with 8-GHz ATCA contours. Contours are chosen at (3, 5, 8, 10, 12, 13, 14, 15)σ. In the radio maps, the white ellipses represent the synthetic beam.

Table 2. Observed flux densities $S_{obs}(\nu)$ at 5.5 and 9 GHz and angular sizes at 9 GHz.

Source	S_{obs}(5.5 GHz) (mJy)	S_{obs}(9 GHz) (mJy)	Angular sizes
S61	2.1 ± 0.1	2.2 ± 0.3	5.1″ × 5.7″
R127	3.1 ± 0.2	3.3 ± 0.4	6.6″ × 7.5″
R143	2.4 ± 0.9	4.0 ± 0.7	3.7″ × 3.2″
S119	1.0 ± 0.2	0.9 ± 0.2	8.0″ × 9.6″ [a]

[a] From the map at 5.5 GHz.

The morphology in the radio map is quite similar to the optical one. The overlay with the optical image (Fig. 1, bottom panel) show that the nebula might be contaminated by the nearby 30 Dor H II region emission, as is the optical one.

Unresolved compact emission at the position of the star is also visible in the map at 9 GHz.

S119 was proposed by Nota et al. (1994) as a LBV candidate after the discovery of a nebula around the previously classified Ofpe/WN9 star (Bohannan & Walborn 1989). The nebula appeared as a shell with a brighter lobe in the north-east direction (Nota et al. 1994). With the *HST* high-resolution image, Weis et al. (2003) detected small-scale structures such as filaments and knots, which give the nebula a patchy appearance.

The marked asymmetry of the nebula was explained (Danforth & Chu 2001) as due to a bow-shock interaction with the interstellar medium (ISM), since the S119 radial velocity (blueshifted ~100 km s^{-1} from the LMC systemic velocity: Nota et al. 1994) suggests a runaway nature for the star.

The diffuse emission visible at 6 cm above 3σ (green/blue levels in the online version of Fig. 1, top panel) is not detected at ATCA 3 cm, but the thicker north-east and south-east parts are well detected and resemble the Hα morphology. In particular the south-east compact region (circle 'a' in the figure) is not visible at the lower frequency. This might be due to the presence of an optically thick H II region. We can speculate that this is the result of an interaction between the stellar ejecta and the close ISM.

4 DATA ANALYSIS

4.1 Intrinsic extinction and spectral index

Under typical conditions of the ISM, the optical emission can be affected by extinction due to dust, while radio emission is not. We can establish whether the optical emission of ionized nebulae is affected by intrinsic extinction, following one of the methods for measuring extinction described by Pottasch (1984). This consists of a comparison between the recombination hydrogen line and the radio continuum emission coefficients (which have the same dependence on the nebular density) through the following relation:

$$S_\nu = 2.51 \times 10^7 T_e^{0.53} \nu^{-0.1} Y F(H\beta)_{exp} \quad [\text{Jy}], \tag{1}$$

where T_e is the electron temperature of the nebula in units of K, ν is the radio frequency in GHz, Y is a factor incorporating the ionized He/H ratios,

$$Y = 1 + \frac{n(He^+)}{n(H^+)} + 4\frac{n(He^{++})}{n(H^+)}\frac{\ln(4.95 \times 10^{-2} T_e^{3/2} \nu^{-1})}{\ln(9.9 \times 10^{-2} T_e^{3/2} \nu^{-1})}, \tag{2}$$

and $F(H\beta)_{exp}$ is the expected Hβ flux when the nebula is not affected by intrinsic extinction. For a nebula with electron density less than 10^4 cm^{-3} and electron temperature ~10^4 K, $F(H\beta)_{exp} =$

Table 3. Electron density n_e, electron temperature T_e and effective temperature T_{eff} available in the literature.

Source	n_e (cm^{-3})	T_e (K)	T_{eff} (K)
S61	400[a]	6120[a]	27600[c]
R127	720[b]	6420 ± 300[b]	16000[d]
R143	1000[b]	12200 ± 1500[b]	9700[e]
S119	680[b]	<6800[b]	26200[c]

[a] Pasquali et al. (1999)
[b] Smith et al. (1998)
[c] Crowther & Smith (1997)
[d] Stahl et al. (1983)
[e] Davies et al. (2005)

Table 4. Hα line integrated flux $F(H\alpha)$ and expected free–free density flux $S_{exp}(\nu)$.

Source	$F(H\alpha)$ (10^{-14} erg cm^{-2} s^{-1})	S_{exp}(5.5 GHz) (mJy)	S_{exp}(9 GHz) (mJy)
S61	10.6 ± 0.7	1.7 ± 0.1	1.6 ± 0.1
R127	20.0 ± 1.7	3.3 ± 0.3	3.2 ± 0.3
R143	3.6 ± 2.1	0.84 ± 0.50	0.80 ± 0.48
S119	6.7 ± 0.7	1.14 ± 0.11	1.09 ± 0.11

$F(H\alpha)_{exp}/2.85$ (see table III-1 in Pottasch 1984). To evaluate the second term in equation (2), we consider that in a low-ionization nebula (see T_{eff} in Table 3), where the ionization is due mainly to the radiation field of the star, and with small $n(He)/n(H)$ ratios (typically 0.1–0.2 in the nebula, e.g. Lamers et al. 2001), the contribution from $n(He^+)$ to the free–free emission is negligible and consequently also the contribution from $n(He^{++})$.

Hence from the *HST* images we have measured the flux emitted in Hα. We have extracted aperture photometry fitting a circle around the star and another around the nebula. For R143, which does not have a rounded shape, we used a polygonal line to select the region in which to measure the flux density. Since we are interested in the recombination-line emission of the ionized nebulae, we have substituted the stellar contribution with the mean brightness around the star. In the case of R127 we have also subtracted the contribution from the external star projected on the nebula. Fluxes in Hα are reported in Table 4.

We have measured the radio flux densities, integrating over the entire nebula, by using an interactive tool of CASA. The root-mean-square rms noise σ has been evaluated far from the targets. Flux densities were therefore compared with the sum of the clean components inside the regions. Since both measures are consistent with each other, we report the values measured with the interactive mode in Table 2. Flux-density errors are defined as $\epsilon = \sigma\sqrt{N}$, where N is the number of independent beams in the selected region (Brogan et al. 2006). The error due to calibration uncertainty[3] is not taken into account.

Finally, with $Y = 1$ and using as T_e the values found in the literature (Table 3), from the measured Hα we have estimated the radio fluxes at the observed frequencies (Table 4) and compared these with the observed ones (Table 2).

The angular resolution obtained is not sufficient to isolate stellar objects. Evidence of stellar wind comes from the positive value of

[3] <10 per cent for 1934−638.

Table 5. Spectral index $\alpha_{\rm obs}$, emission measure $\langle {\rm EM} \rangle$, linear size, geometrical depth s, source solid angle Ω_s, average electron density $\langle n_{\rm e} \rangle$ and ionized mass $M_{\rm ionized}$.

Source	$\alpha_{\rm obs}$	$\langle {\rm EM} \rangle$ [pc cm^{-6}]	Linear size (pc × pc)	s (pc)	Ω_s (arcsec)^2	$\langle n_{\rm e} \rangle$ (cm^{-3})	$M_{\rm ionized}$ (M$_\odot$)
S61	0.1	1364	1.2 × 1.3	0.40	24.5	58	0.78
R127	0.1	1345	1.6 × 1.8	0.28–0.59	38.1	69–48	1.01–1.46
R143	1.0	1697	0.9 × 0.8	0.24–0.71	19	85–49	0.52–0.90
S119	-0.2 [a]	222	1.9 × 2.3	0.61	71	19	1.13

[a] This value must be considered a lower limit.

spectral indices α (Table 5), which indicates a contribution to the nebular free–free optically thin emission that is more important at higher frequencies. Despite this, the values that we found indicate that the Hα emission probably does not suffer from strong intrinsic extinction. This is apparently true for both R127 and S119, which have density fluxes equal to the expected ones within the errors. Moreover, for R127 we have evidence of a stellar wind contribution at 9 GHz. In the case of S119 we cannot assess this because of the sensitivity limit at 9 GHz.

A similar discussion on the central object contribution can be applied to S61 and R143, even if in the last case the spectral index evidently shows that the nebula flux is contaminated by other emission sources (i.e. 30 Dor H II region). Moreover we cannot exclude the presence of dust in the vicinity, which may cause optical extinction.

The S61 flux densities at both 5.5 and 9 GHz are higher than the values expected from recombination-line flux estimation. This could be due to an important stellar wind contribution even at the lowest frequencies or to a non-negligible dusty nebular component.

4.2 Mass of the ionized nebula

From the radio free–free emission measurement we can estimate the total ionized mass as the total amount of particles present in the nebula. For non-self-absorbed free–free emission, the electron density in a nebula can be determined through the relation between the emission measure,

$$\mathrm{EM} = \int_0^s n_{\rm e}^2 \, \mathrm{d}l \quad [{\rm pc \ cm}^{-6}], \tag{3}$$

and the optical depth $\tau_{\rm ff}$,

$$\tau_{\rm ff} = 8.24 \times 10^{-2} T_{\rm e}^{-1.35} \left(\frac{\nu_{\rm [GHz]}}{5} \right)^{-2.1} {\rm EM}, \tag{4}$$

where $\tau_{\rm ff}$ is evaluated for each pixel from the observed brightness B_ν which, in the optically thin case, is $B_\nu = B(T)\tau$, where $B(T)$ is a blackbody with an assumed temperature T equal to the gas temperature $T_{\rm e}$ (see Table 3).

From the mean $\langle {\rm EM} \rangle$ measured in the map, by inverting equation (3), it is possible to estimate a mean value for the particle density $\langle n_{\rm e} \rangle$. Assuming that nebulae are uniform, the emission measure is simply ${\rm EM} = \langle n_{\rm e} \rangle^2 s$, where the geometrical depth s needs a strong hypothesis regarding nebular geometries.

It has generally been believed that LBVNe are often torus-like, indicating that mass loss happens in a preferred direction (e.g. Clark et al. 2003; Davies, Oudmaijer & Vink 2005). If this is true, the nebulae associated with R127, S61 and S119 may be tori seen pole-on and that of R143 may be seen roughly edge-on. Hence we assume a depth equal to the transversal size measured on the maps, chosen where the emission is 70 per cent of the peak flux density (as shown with white lines in Fig. 1). In the cases of R127 and R143

we calculated the electron density and the ionized mass assuming two different geometrical depths (1.2 and 2.5 arcsec for R127, 1 and 3 arcsec for R143).

Finally, the total ionized mass is given by the total amount of particles in the nebula, i.e. by $M_{\rm ionized} = \langle n_{\rm e} \rangle (m_{\rm p}/{\rm M}_\odot)V$. The volume assumed for each nebula is given by the area over which we have estimated the $\langle {\rm EM} \rangle$ and the assumed geometrical depths. The resulting masses are reported in Table 5, together with the other physical parameters. The linear sizes in the table are obtained assuming for nebulae the distance of the LMC ($D = 48.5$ kpc).

From our estimation, the masses range between 0.5 and 1.5 M$_\odot$, which are typical values for nebular masses of Galactic LBVs (in general, a few solar masses: Humphreys & Davidson 1994; Clark et al. 2005).

5 DISCUSSION/CONCLUSIONS

The improved sensitivity at ATCA with the new CABB correlator has allowed us to obtain the first radio detections of the nebulae around four LBV-type stars in the Large Magellanic Cloud. Even if our highest resolution cannot distinguish angular scales smaller than 1.5 arcsec (that means structures of linear sizes ~ 0.35 pc at a distance of 48.5 kpc), it was possible to measure nebular sizes and to compare the radio morphology with the optical one. The linear sizes are consistent with previous estimates at different wavelengths (Hα: Weis 2003; Weis et al. 2003) as well as with Galactic examples (e.g. Clark et al. 2003). No evident differences are visible, as expected if the Hα is not intrinsically extinguished. On the contrary, the radio resembles the optical. A similar result was found by Duncan & White (2002), studying four Galactic LBVNe and comparing the radio images with the Hα ones. This strict similarity was particularly evident in AG Car.

The radio flux densities were compared here with the extrapolated fluxes from the recombination hydrogen line. The *HST* Hα-equivalent filter F656N has a bandwidth ≈ 28 Å, with the Hα line in the band centre, and does not cover Hα velocity features higher in magnitude than 640 km s^{-1}. However, high-resolution Echelle spectra in Weis (2003) showed that high-velocity outflows are not present in such nebulae. On the other hand, the filter can detect the signal from [N II] 6548-Å emission. Assuming a mean value for [N II]6584-Å/Hα (0.6, Smith et al. 1998) and that this is valid also for the [N II] 6548-Å line, and considering that the filter response at 6548 Å is about 25 per cent of the maximum, then the Hα emission evaluated here may be overestimated by 15 per cent and thus has to be considered an upper limit.

Such contamination of Hα due to [N II] is, however, within the flux errors for most of our sources. If we assume that all the flux falling in the filter is due to Hα, comparison between the radio and optical fluxes does not show any differences and this leads us to suppose that there is no intrinsic extinction, especially in the cases

of R127 and S119. On the other hand, if there were some extinction this would be attributable to uniformly distributed dust, as the radio morphology resembles the optical one and we may exclude any clumping in the dust distribution.

A similar discussion must be performed with caution in the case of S61, the optical emission of which could be affected by intrinsic extinction due to dust, and in the case of R143, which is probably affected by emission from the close H II region as well as a likely dusty environment.

The derived spectral indices indicate a possible contribution from a central object that must be considered and, more specifically, show that current mass loss from the central star is ongoing.

In addition, values for the ionized mass have been obtained in this work. Estimates for the nebular mass of S119 and R127 have been previously reported. In particular, Nota et al. (1994) and Clampin et al. (1993) provided a mass of $M = 1.7\,\mathrm{M_\odot}$ for the nebula of S119 and $M = 3.1\,\mathrm{M_\odot}$ for R127. These results were obtained by integrating Hα emission luminosity and adopting values for the electron density of the order of 800–1000 cm^{-3}, derived from the [S II 6716/6731]-Å line ratio, and a temperature of 7500 K. A further value for the mass of R127 was found by Munari et al. (2009) through photoionization modelling of the emission-line spectrum in the range 8400–8800 Å. They found a mass of $1.33 \times 10^{-3}\,\mathrm{M_\odot}$.

We are conscious that the ionized mass estimated with this method is very sensible to the assumed geometry and that we are not taking into account the filling factor correction. If these circumstellar nebulae are not homogeneous as we assumed then the true average density and hence the nebular masses are smaller than the estimates provided here, by the value of the filling factor (typically between ∼0.2–0.7 for extended nebulae, e.g. Mallik & Peimbert 1988; Boffi & Stanghellini 1994). Both these facts may lead to a discrepancy with the measurements reported in table 9 of Clark et al. (2003).

The contribution from the stellar wind to the total emission can be neglected. In fact, assuming a mass-loss rate of $\dot{M} \sim 10^{-5}\,\mathrm{M_\odot}\,\mathrm{yr}^{-1}$ and a stellar wind velocity of $v_\infty \sim 100\,\mathrm{km\,s}^{-1}$, which are typical values for Galactic LBVs, the flux density due to the stellar wind will be of the order of 0.03 mJy at 9 GHz (Panagia & Felli 1975), i.e. only 1 per cent of the observed flux density. This means that the overestimation of the mean electron density and the ionized mass are negligible. In the case of R143, an overestimation could be assigned to the close H II region emission. The values reported here must, then, be considered only as indicative, but are almost consistent with the values in Clampin et al. (1993) and Nota et al. (1994).

Thanks to its properties, radio emission can be used as a good probe of the ionized gas emission from a nebula around a hot star. This is important when one wants to determine the gas content to establish the total mass budget ejected during the LBV phase and to constrain stellar evolution models of very massive stars. For the moment, the resolution achieved at ATCA in this work does not allow us to separate the nebular and stellar contributions to the total emission.

To resolve this issue, new higher resolution observations can provide a more detailed morphological study of the nebula, as well as a possible detection of the central stellar wind and hence the current mass-loss rate, where the optical Hα estimates can be uncertain.

ACKNOWLEDGMENTS

REFERENCES

Boffi F. R., Stanghellini L., 1994, A&A, 284, 248
Bohannan B., Walborn N. R., 1989, PASP, 101, 520
Brogan C. L., Gelfand J. D., Gaensler B. M., Kassim N. E., Lazio T. J. W., 2006, ApJ, 639, L25
Buemi C. S., Umana G., Trigilio C., Leto P., Hora J. L., 2010, ApJ, 721, 1404
Clampin M., Nota A., Golimowski D. A., Leitherer C., Durrance S. T., 1993, ApJ, 410, L35
Clark B. G., 1980, A&A, 89, 377
Clark J. S., Egan M. P., Crowther P. A., Mizuno D. R., Larionov V. M., Arkharov A., 2003, A&A, 412, 185
Clark J. S., Larionov V. M., Arkharov A., 2005, A&A, 435, 239
Crowther P. A., Smith L. J., 1997, A&A, 320, 500
Danforth C. W., Chu Y.-H., 2001, ApJ, 552, L155
Davies B., Oudmaijer R. D., Vink J. S., 2005, A&A, 439, 1107
Duncan R. A., White S. M., 2002, MNRAS, 330, 63
Feast M. W., 1961, MNRAS, 122, 1
Humphreys R. M., Davidson K., 1994, PASP, 106, 1025
Jiménez-Esteban F. M., Rizzo J. R., Palau A., 2010, ApJ, 713, 429
Lamers H. J. G. L. M., Nota A., Panagia N., Smith L. J., Langer N., 2001, ApJ, 551, 764
Mallik D. C. V., Peimbert M., 1988, Rev. Mex. Astron. Astrofis., 16, 111
Munari U. et al., 2009, A&A, 503, 511
Nota A., Drissen L., Clampin M., Leitherer C., Pasquali A., Robert C., Paresce F., Robberto M., 1994, in Clegg R., ed., Circumstellar Media in the Late Stages of Stellar Evolution. Cambridge Univ. Press, Cambridge, p. 89
Panagia N., Felli M., 1975, A&A, 39, 1
Parker J. W., Clayton G. C., Winge C., Conti P. S., 1993, ApJ, 409, 770
Pasquali A., Nota A., Clampin M., 1999, A&A, 343, 536
Pottasch S. R., 1984, Planetary Nebulae: A Study of Late Stages of Stellar Evolution. Reidel, Dordrecht
Sault R. J., Teuben P. J., Wright M. C. H., 1995, in Shaw R. A., Payne H. E., Hayes J. J. E., eds, ASP Conf. Ser. Vol. 77, Astronomical Data Analysis Software and Systems IV. Astron. Soc. Pac., San Francisco, p. 433
Smith N., Owocki S. P., 2006, ApJ, 645, L45
Smith L. J., Nota A., Pasquali A., Leitherer C., Clampin M., Crowther P. A., 1998, ApJ, 503, 278
Stahl O., Wolf B., Klare G., Cassatella A., Krautter J., Persi P., Ferrari-Toniolo M., 1983, A&A, 127, 49
Umana G., Buemi C. S., Trigilio C., Leto P., Hora J. L., 2010, ApJ, 718, 1036
Umana G., Buemi C. S., Trigilio C., Leto P., Hora J. L., Fazio G., 2011a, Bull. Soc. Royale des Sciences de Liege, 80, 335
Umana G., Buemi C. S., Trigilio C., Leto P., Agliozzo C., Ingallinera A., Noriega-Crespo A., Hora J. L., 2011b, ApJ, 739, L11
van Genderen A. M., 2001, A&A, 366, 508
Walborn N. R., 1977, ApJ, 215, 53
Walborn N. R., 1982, ApJ, 256, 452
Weis K., 2003, A&A, 408, 205
Weis K., Duschl W. J., Bomans D. J., 2003, A&A, 398, 1041
Zacharias N., Monet D. G., Levine S. E., Urban S. E., Gaume R., Wycoff G. L., 2005, VizieR Online Data Catalog, 1297, 0

This paper has been typeset from a TEX/LATEX file prepared by the author.